How the capillary burst microvalve works. J Colloid Interface Sci

ARTICLE *in* JOURNAL OF COLLOID AND INTERFACE SCIENCE · MARCH 2007

Impact Factor: 3.37 · DOI: 10.1016/j.jcis.2006.10.077 · Source: PubMed

4 AUTHORS, INCLUDING:

Hansang Cho
University of North Carolina at Charlotte
25 PUBLICATIONS **367** CITATIONS
SEE PROFILE

Ji Yoon Kang
Korea Institute of Science and Technology
178 PUBLICATIONS **2,404** CITATIONS
SEE PROFILE

Available online at www.sciencedirect.com
ScienceDirect
Journal of Colloid and Interface Science 306 (2007) 379–385
JOURNAL OF Colloid and Interface Science
www.elsevier.com/locate/jcis

How the capillary burst microvalve works

Hansang Cho [a,c], Ho-Young Kim [b], Ji Yoon Kang [c], Tae Song Kim [c,*]

[a] *Berkeley Sensor and Actuator Center, Department of Bioengineering, University of California, Berkeley, CA 94720, USA*
[b] *School of Mechanical and Aerospace Engineering, Seoul National University, Seoul 151-744, Republic of Korea*
[c] *Microsystem Research Center, Korea Institute of Science and Technology, Seoul 136-791, Republic of Korea*

Received 14 August 2006; accepted 25 October 2006

Available online 3 November 2006

Abstract

The capillary burst microvalve offers an attractive means to regulate microliquid flow owing to its simple structure and operation process. However, there existed no rigorous theoretical work to elucidate how the valve works and consequently to predict the valve-bursting condition. Therefore, here we report the theoretical investigation of how the capillary burst valve can stop the advancing liquid meniscus and when it bursts. We confirm our theory with experiments using a centrifugal microfluidic valve system fabricated by soft lithography.

Keywords: Capillary burst valve; Microfluidics; Contact angle; Interface; Wetting; Surface tension

1. Introduction

It is currently of a great interest to integrate microfluidic systems for biochemical analysis with other functional components, such as sensors and reaction chambers [1–4]. The major advantage of the integrated microfluidic systems is that they consume only a minute amount of biochemical fluid while keeping a high sensitivity. Hence they are expected to be widely used in many applications including proteomics, rapid drug screening, and portable disease-detecting or therapeutic systems. The microfluidic systems are mainly composed of micropumps, microvalves and microchannels. It is difficult to integrate such components of microscales with other biochemical components such as sensors and catalytic device fabricated by different processes and made of different materials. Therefore, simplifying the design and fabrication process of microfluidic systems is crucial in achieving the integration of various functional parts.

Recently, simple driving and regulating systems for microliquid flow have been suggested to substitute for such complex handling systems as those based on piezoelectric materials [5] and electrokinetics [6]. The focus of this work is on the flow-regulating device that involves no complex design and fabrication processes. One of the candidates is the capillary burst valve (referred to as CBV hereafter) that regulates the liquid flow only by giving a microchannel a simple geometric or surface-chemical variation. The geometrical CBV designates a sudden expansion of the microchannel where the liquid meniscus is trapped at the beginning of the expansion. The surface-chemical CBV stops the liquid flow where the sudden change of the wetting properties occurs [7]. In either case, the liquid meniscus is stopped at the valve until the driving force overcomes the resisting capillary force, thus the flow regulation is easily achieved by controlling the driving force. When the valve bursts, the remaining channel is wetted by advancing liquid.

Here we consider the geometric CBV that involves no chemical treatment. The concept of the geometric CBV was suggested and tested earlier [8,9]. The most important performance measure of the valve is how much pressure it can withstand before bursting. In that aspect, earlier researchers showed that the bursting pressure of the geometric CBV is proportional to the surface tension of liquid and inversely proportional to the channel dimension. However, no further rigorous theoretical development was made to determine the empirical constants appearing in their empirical relationship for the maximum pressure difference that the valve can withstand [10]. Therefore,

* Corresponding author. Fax: +822 958 6910.
E-mail address: tskim@microsystem.re.kr (T.S. Kim).

0021-9797/$ – see front matter
doi:10.1016/j.jcis.2006.10.077

here we aim to elucidate the fundamental working principle of the geometrical CBV and propose the relationship of the maximum pressure to the valve dimensions and the liquid properties.

We first start with a brief introduction of the basic theory of contact line movement needed for the problem of geometric CBV. Then we thoroughly analyze the working principle of the valve to predict the bursting condition of the valve both in circular and rectangular channels. We then compare the theoretical results with the experimental measurements using a centrifugal microfluidic valve system fabricated by soft lithography [11].

2. Theoretical analysis

2.1. Theory for a round tube

We consider a circular tube meeting an abruptly diverging section as shown in Fig. 1 as the simplest geometry. When the liquid meniscus is in the straight section, the pressure jump, i.e., the difference between the pressure inside and outside the liquid, P_A and P_o, respectively, under equilibrium is given by the Young–Laplace equation, $\Delta P_e = P_A - P_o = -4\sigma\cos\theta_e/D$, where σ is the surface tension, θ_e the equilibrium contact angle, and D the tube diameter. When θ_e is less than the right angle (hydrophilic wall), spontaneous imbibition occurs until the meniscus meets the diverging section. In this case, $|\Delta P_e|$ is merely the magnitude of pressure difference that drives imbibition. When θ_e is greater than the right angle (hydrophobic wall), the meniscus can only be advanced when the external driving pressure pushes the liquid into the tube. Here we show that the capillary burst valve can work when the channel wall is hydrophobic as well as hydrophilic, contrary to the explanation in [12].

Before investigating the bursting condition, it is necessary to review the theory of contact line motion. As we tilt an initially horizontal solid surface on which a liquid drop is placed, the contact angle of the drop's front edge increases. While the front contact line is stationary before the drop starts to slide down, the static contact angle keeps increasing [13–15]. The contact angle at which the contact line starts to move is termed the critical advancing contact angle, θ_A. The contact line cannot advance when its contact angle is less than the critical advancing contact angle which is greater than the equilibrium contact angle: $\theta_e < \theta_A$. When the meniscus is in motion, the apparent dynamic contact angle, θ_a, is dependent on the contact line velocity, U, as well as the critical contact angle, in general: $\theta_a = f(U, \theta_A)$. It is known that for small capillary number $Ca = \mu U/\sigma < 10^{-3}$, θ_a and θ_A are similar [15] and this will be assumed in the following. Hence the apparent contact angle should be greater than θ_e when the liquid meniscus advances in the straight channel. Therefore, the minimum pressure difference needed to advance the liquid interface is given by $\Delta P_a = -4\sigma\cos\theta_A/D$ which is greater than ΔP_e.

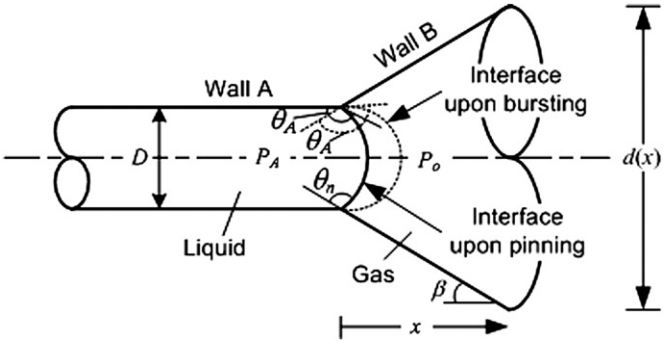

Fig. 1. Capillary burst valve in a round tube.

Now we consider the contact angle that the meniscus forms with a suddenly diverging section. The contact angle that the interface assumes with a new wall (wall B in Fig. 1) is now reduced to $\theta_n = \theta_A - \beta$. Then the contact line stops instantly because the contact angle θ_n is smaller than θ_A. For the contact line to resume advancing, i.e., for the valve to burst, the interface should bulge until the contact angle with the new wall, θ_n, increases to θ_A. In the meantime, the contact angle with the old wall (A in the figure) θ_I increases from θ_A to $\theta_A + \beta$. This picture is consistent with the model for resistance to liquid spreading due to sharp solid edges originally proposed by Gibbs [16,17]. It should also be noted that the maximum contact angle that a liquid meniscus can attain is 180°. Thus for $\theta_A + \beta > 180°$, the valve bursts when θ_I reaches 180°. The Young–Laplace equation for the bulging interface gives the pressure difference as $P_A - P_o = -4\sigma\cos\theta_I/D$. This pressure difference is always greater than ΔP_a whether the channel is hydrophilic or hydrophobic. Hence the meniscus is kept pinned until the driving pressure becomes large enough to overcome the maximum pressure difference that the bulging interface can withstand. Such maximum pressure difference is obtained by substituting $\theta_I^* = \min\{\theta_A + \beta, 180°\}$ for θ_I. Upon the valve bursting, the liquid interface advances along the diverging wall and its curvature keeps decreasing. The pressure difference across the interface in the post-pinned state is given by $P_A - P_o = -4\sigma\cos\theta_I^*/d(x)$. It can be readily shown that the foregoing argument holds when the wall is hydrophilic ($\theta_A < 90°$) as well. We again emphasize that the capillary burst valve can regulate liquid flow when the channel wall is hydrophobic as well as hydrophilic.

2.2. Theory for a rectangular channel

In this section, we consider the liquid interface in a rectangular channel. In a case the liquid has the advancing contact angle θ_s with the sidewall and θ_v with the top and bottom walls, the Young–Laplace equation yields

$$P_A - P_o = -2\sigma\left(\frac{\cos\theta_s}{w} + \frac{\cos\theta_v}{h}\right), \tag{1}$$

where w and h are the width and the height of the channel, respectively. For the interface to advance, we assume that the following should be satisfied: $\theta_s \geqslant \theta_A$ and $\theta_v \geqslant \theta_A$. Now we consider the pressure difference when the interface meets a suddenly diverging channel section as shown in Fig. 2. The contact line at the sidewall stops instantly because the contact angle that the interface assumes with a new sidewall (B in the figure) is now reduced to $\theta_n = \theta_s - \beta$. As in the round tube, the

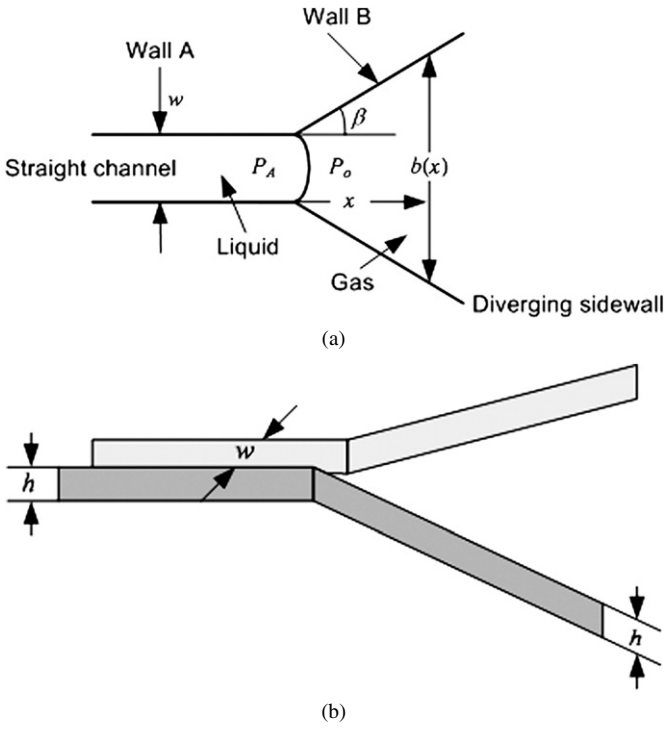

Fig. 2. Capillary burst valve in a rectangular channel. (a) Top view. (b) Bird's eye view.

interface bulges before resuming its advance, thus the contact angle with the old sidewall (A in the figure) θ_I increases from θ_A to $\min\{\theta_A + \beta, 180°\}$. The Young–Laplace equation for the bulging interface gives the pressure difference as

$$P_A - P_o = -2\sigma\left(\frac{\cos\theta_I}{w} + \frac{\cos\theta_A}{h}\right), \tag{2}$$

where θ_s of Eq. (1) has been replaced by θ_I. We have also replaced θ_v by θ_A. The maximum pressure difference that the valve can withstand is obtained by substituting $\theta_I^* = \min\{\theta_A + \beta, 180°\}$ for θ_I in Eq. (2). Upon the valve bursting, the liquid interface advances along the diverging sidewall and its curvature keeps decreasing. The pressure difference across the static interface in a post-pinned state, is given by

$$P_A - P_o = -2\sigma\left[\frac{\cos\theta_I^*}{b} + \frac{\cos\theta_A}{h}\right], \tag{3}$$

where b denotes the width of the diverging section. Fig. 3 shows the pressure profile depending on the location of the contact line. Until the pressure difference reaches the threshold value, the contact line is pinned. Once the valve bursts, the meniscus advances into the valve area, where lower pressure difference is required for movement, exhibiting an abrupt "bursting" motion.

2.3. Bursting condition for a slug of finite length

So far we have considered the liquid flow having the advancing meniscus and infinite reservoir in the rear. For a finite amount of liquid, the receding interface exists as illustrated in Fig. 4. For the static rear interface, the Young–Laplace equation

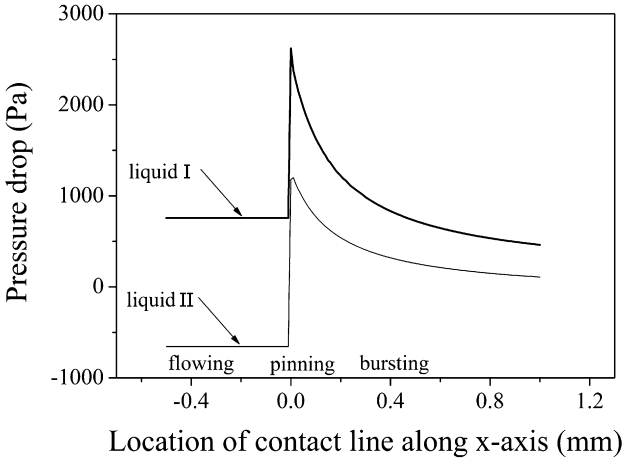

Fig. 3. The theoretical pressure profile versus the contact line location. The pressure builds up at the valve edge and it drops as soon as the valve bursts. The channel and valve (PDMS) dimensions are such that $w = 60$ μm, $h = 150$ μm and $\beta = 120°$. The liquid properties are listed in Table 1.

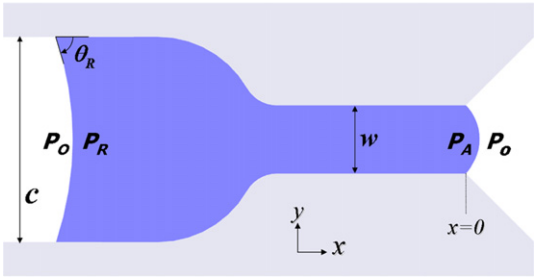

Fig. 4. The top view of a finite volume of liquid flowing to the right in a microchannel.

again gives the following pressure difference:

$$P_R - P_o = -2\sigma\left(\frac{\cos\theta_R}{c} + \frac{\cos\theta_R}{h}\right), \tag{4}$$

where P_R is the liquid pressure inside the rear interface and c the width of the rear interface. The rear meniscus starts to recede as the contact angle becomes smaller than the critical receding contact angle, θ_R. Therefore, for a liquid slug having both the advancing and receding fronts to move, the driving pressure should overcome the following pressure difference:

$$\begin{aligned}\Delta P &= P_A - P_R \\ &= -2\sigma\left[\frac{\cos\bar{\theta}_I}{w} - \frac{\cos\theta_R}{c} + \frac{(\cos\theta_A - \cos\theta_R)}{h}\right].\end{aligned} \tag{5}$$

For a slug advancing in a straight channel, $\bar{\theta}_I$ in Eq. (5) is replaced by θ_A, while for a slug blocked by the capillary burst valve, $\bar{\theta}_I$ is replaced by θ_I^*.

In the following, we experimentally investigate the validity of our theory. In the experiments, we employ a rotating system where the centrifugal force drives the liquid flow [8]. Thus the driving pressure, ΔP_d, exerted on the liquid slug, whose receding and advancing fronts are located r_1 and r_2 from the rotation center, respectively, is given by

$$\Delta P_d = \frac{1}{2}\rho\omega^2\left(r_2^2 - r_1^2\right), \tag{6}$$

where ρ is the density of the liquid and ω the angular velocity. Then we obtain the following angular velocity, ω_b, causing the valve to burst:

$$\omega_b = \left[4\sigma \frac{(\cos\theta_R - \cos\theta_A)/h + (\cos\theta_R/c - \cos\theta_I^*/w)}{\rho(r_2^2 - r_1^2)}\right]^{1/2}. \tag{7}$$

3. Experiments

We fabricated the microchannel having the capillary burst valve by means of soft lithography. The fabrication process is illustrated in Fig. 5. A 150 μm-thick negative photoresist (SU-8 100, Microchem, corp.) was spin-coated onto a silicon substrate, and was left on a flat surface for 10 min for stress relaxation. Then the photoresist was soft-baked at 65 °C for 20 min and at 95 °C for 50 min on a hotplate. UV (ultraviolet) exposure was carried out with a dose of 255 mJ/cm^2 and a post-exposure bake was performed at 65 °C for 1 min and 95 °C for 12 min. A care was taken during each baking and cooling process to minimize thermal stress of the photoresist due to a rapid temperature gradient. The thermal stress tends to be concentrated at the opening edge of the valve, eventually deforming the microstructure. The fabricated mold structure for the valve was observed with a scanning electron microscope (SEM) to check the degree of thermal deformation. Fig. 6 shows the SEM images of the fabricated mold of a valve and a channel. Polydimethylsiloxane (PDMS) was poured on the mold and spun to yield an elastomer replica. The cured PDMS replica of 1 mm in height was cut and bored by laser. The PDMS replica was bonded to a transparent PC (polycarbonate) substrate of 4″ diameter. Before the bonding process, the 10 μm thick primer (Dow Corning) was spin-coated to enhance the adhesion of PDMS to other plastics and was then cured for 1 h at room temperature. On the primer coated surface, a less viscous mixture of PDMS was spin-coated to a thickness of 10 μm and then cured for 1 h at 80 °C. After the surfaces of replica and the coated substrate were treated by oxygen plasma, they were brought into contact and loaded for a day. The image of thus fabricated evaluation disk is presented in Fig. 7. We used channels of different widths ranging from $w = 15$ to 150 μm although the channel height was fixed at 150 μm. For each channel width, three different diverging angles of valves ($\beta = 60°$, 90°, and 120°) were adopted.

The liquids used in the experiments were two mixtures of water and dye (Phenol Red, Sigma–Aldrich) having different physical properties depending on the concentration of the dye as listed in Table 1. The critical advancing and reced-

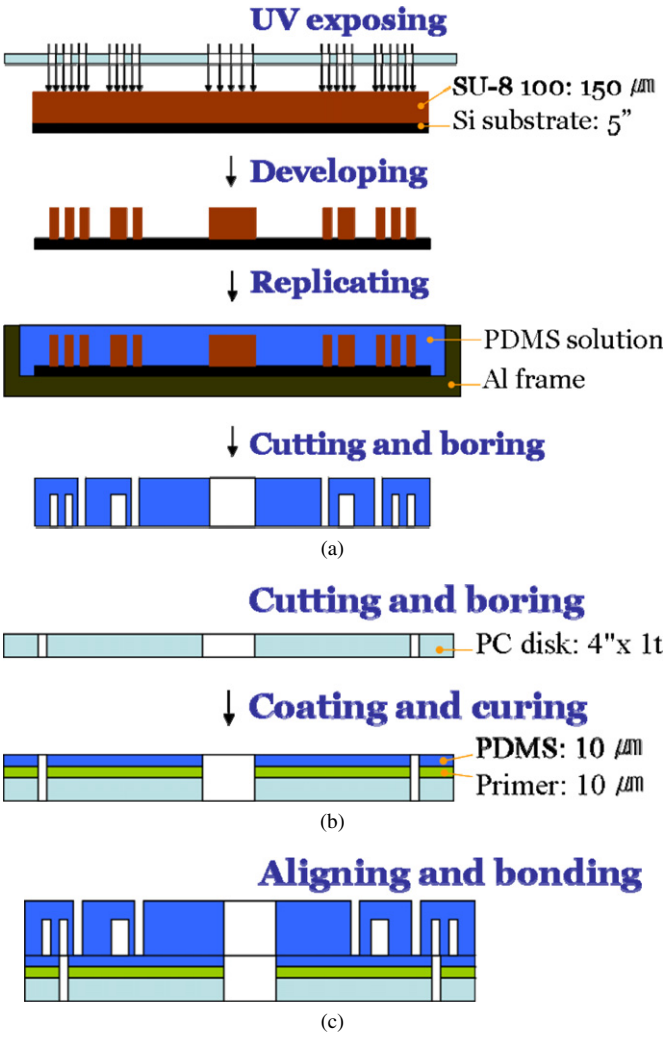

Fig. 5. Fabrication steps of a microfluidic centrifugal disk for microliquid transport. (a) Fabrication process of a PDMS microchannel. (b) Preparation process of a PC (polycarbonate) disk for bonding to a PDMS channel. (c) The microfluidic centrifugal disk prepared by bonding the PDMS channel to the PC disk.

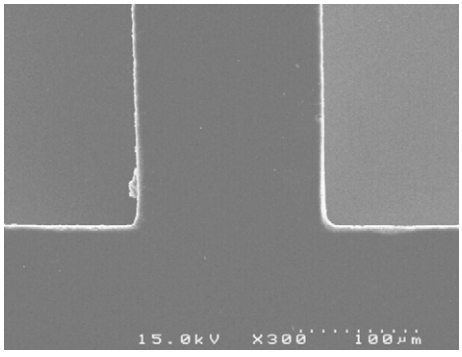

(a)

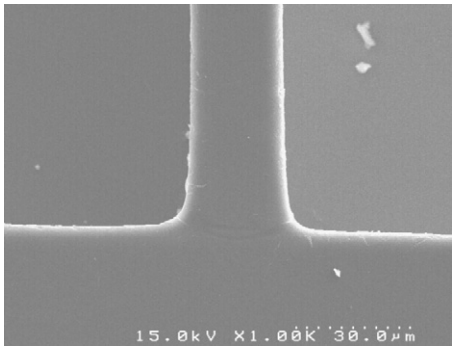

(b)

Fig. 6. SEM images of the SU-8 molds for the channel and the valve. The channel widths are (a) 155 and (b) 20 μm.

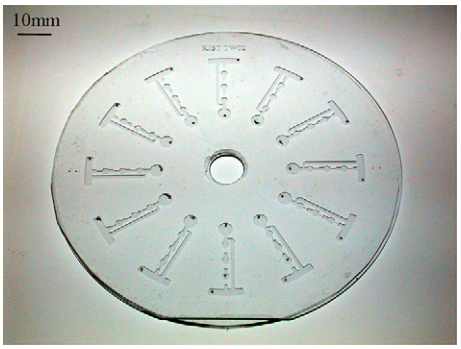

(a)

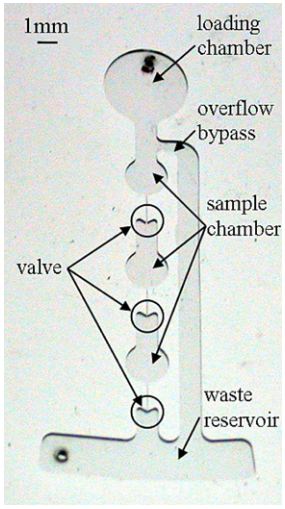

(b)

Fig. 7. Photographs of the microfluidic centrifugal disk. (a) Overview of the disk. (b) Magnified view of a single unit with the descriptions of each part.

Table 1
Physical properties of the liquids

Liquid	Dye concentration (kg/m^3)	Density (kg/m^3)	Surface tension (N/m)	θ_A on PDMS	θ_R on PDMS
I	80	1078	0.049	86°	66°
II	1	999	0.054	118°	88°

ing contact angles of the liquids on PDMS surface were obtained by a contact angle analyzer (Phoenix 450, Surface Electro Optics, Seoul, Korea) with the measurement resolution less than 2°. The surface tension was measured by the Du Nöuy ring method (DST 30, Surface Electro Optics) with the resolution of 0.3 mN/m.

We imaged the microflow in the rapidly rotating system by triggering the CCD camera connected to a frame grabber in a personal computer. A schematic of the experimental setup is shown in Fig. 8. The liquid loaded in the microchannel underwent the following sequential process as the rotational speed increased. The first sample chamber was filled with 20 μl of liquid from a loading chamber about 50 μl in volume, while the surplus was bypassed into a waste reservoir as the disk started to rotate. With the rotational speed increase, the liquid in the sample chamber was driven through a narrow channel. At a lower rotational speed than the bursting speed, the flow was pinned at the valve. The critical pressure difference causing the valve to

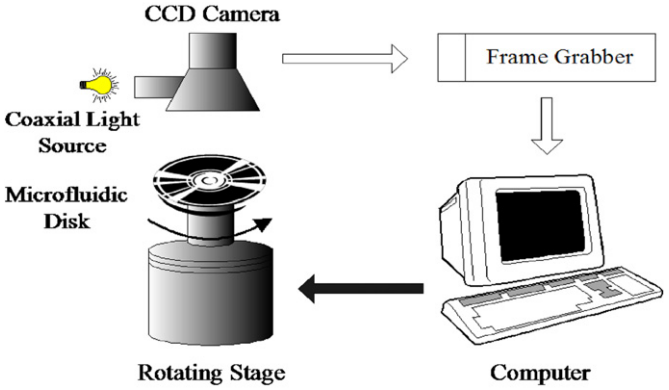

Fig. 8. Schematic of the experimental setup employing the centrifugal microfluidic system and the CCD camera with a high shutter speed.

burst was obtained by gradually increasing the rotational speed. The experimental images corresponding to the aforementioned process are shown in Fig. 9.

4. Results and discussion

Although the centrifugal disk as shown in Fig. 7 has three valves in series for versatile biosample delivery functions, we used a single valve in the experimental measurements reported here. In addition, the valve location, the liquid amount and the rear width were kept constant. Hence we have the following constant values to determine the bursting pressure: $r_1 = 27.5$ mm, $r_2 = 31$ mm and $c = 1$ mm. Therefore, for each liquid/solid combination (θ_A and θ_R) and β, the bursting speed can be plotted as a function of w. The geometric conditions of our valves result in distinct theoretical predictions of the bursting speed versus w, as shown in Fig. 10. In each figure, solid lines correspond to the results of the idealized theoretical model, i.e., Eq. (7), and symbols correspond to the experimental results.

As Fig. 10 shows, the bursting speed, or the maximum driving pressure difference withstood by the capillary burst valve, decreases as the channel width increases. The experimental results are in reasonable agreement with the theoretical predictions for channels wider than 60 μm. When the channel width is less than 40 μm, some data for experimentally measured bursting speed are located below the solid lines. Such discrepancy found in narrow channels can be first attributed to an increasing sensitivity of the bursting speed to the channel width as the width decreases and the difficulty in making a straight channel with sharp edges.

The bursting speed is theoretically inversely proposal to the channel width and therefore the sensitivity of the speed drastically increases as the channel width decreases. For example, the sensitivity at 20 μm channel width for liquid I and II is 155 and 175 rpm/μm, respectively, about 2.7 times that at 65 μm. That is, 1 μm increase of width for a nominal channel width 20 μm may cause decrease of bursting speed by 155 rpm and 175 rpm for liquid I and liquid II, respectively. Therefore, a slight increase of the channel dimension as compared with the original photoresist line width yields a great disadvantage in the valve performance.

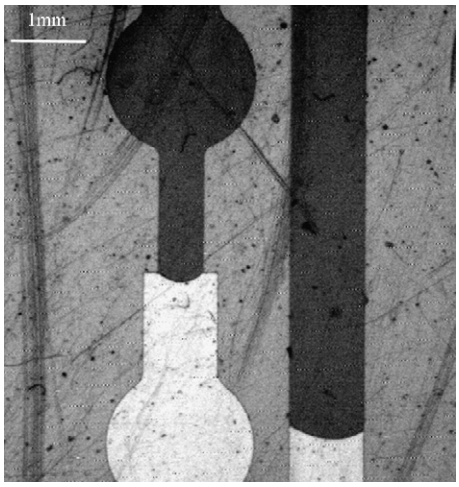

(a)

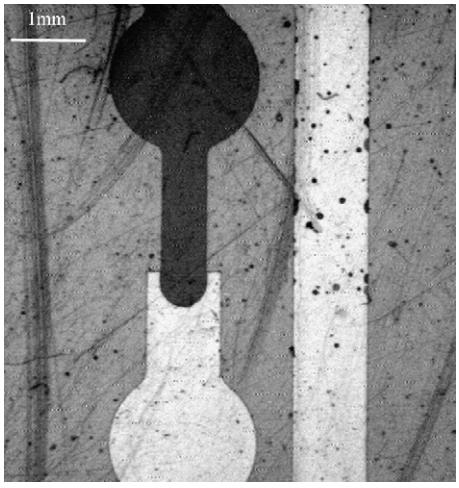

(b)

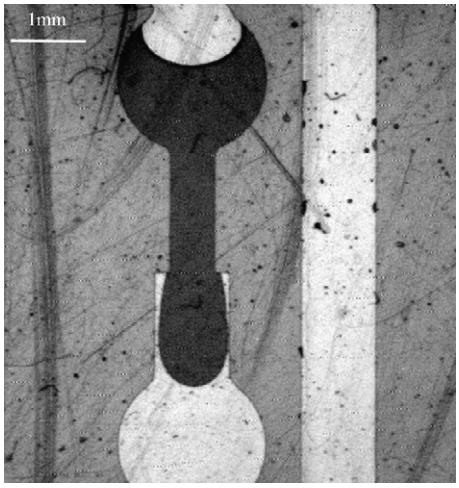

(c)

Fig. 9. Sequential images of the liquid flow around the valve. (a) The meniscus just encountering the valve edge with fluid bypassing through the right channel. (b) The bulged interface about to burst. (c) The liquid invading the valve area after the valve bursting.

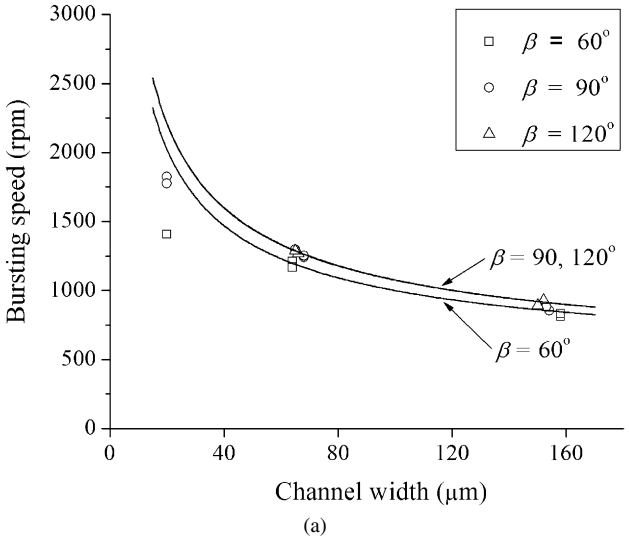

(a)

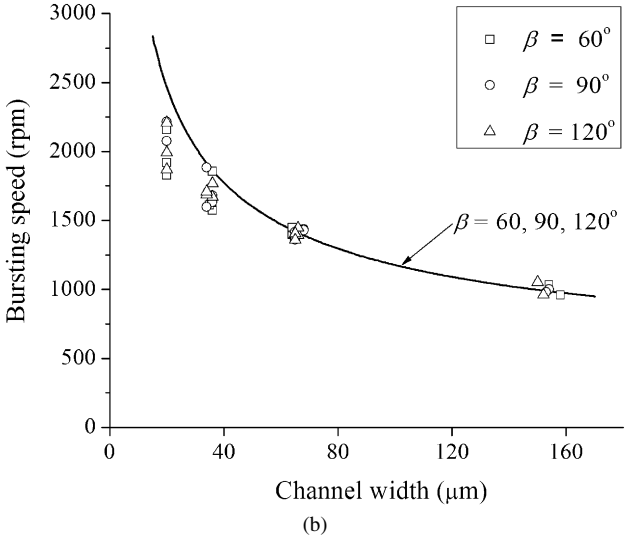

(b)

Fig. 10. Experimental and theoretical results of the valve bursting speed versus the channel width with (a) the liquid I and (b) the liquid II. Solid lines correspond to the results of the idealized theoretical model and symbols correspond to the experimental results. In (a), the theoretical results for $\beta = 90°$ and 120° are indiscernible because $\theta_A + \beta \approx 180°$ ($\beta = 90°$) and $\theta_A + \beta > 180°$ ($\beta = 120°$). In (b), all the theoretical bursting speeds are identical for all the given values of β because $\theta_A + \beta > 180°$.

During fabrication, a thin wall of SU-8, being a mold for the PDMS channel later, tends to warp and reflow upon baking. Consequently, the actual valve-opening angle became lower, and sharp edges where the straight channel and the diverging section meet, became more rounded than the original design (see Fig. 6b). At rounded edges as illustrated in Fig. 11, the opening angle increases gradually from zero to β, implying the gradual increase of pressure difference that blocks the flow. On the other hand, the channel width increases with the opening angle, which tends to decrease the pressure difference. Therefore, the maximum pressure that the valve with a round edge can withstand, which is lower than that with a sharp edge, may take place before the opening angle reaches β. In the real case, the radius of the curvature, $r_e = 10$ μm at 20 μm channel width for liquid I and II might cause a decrease of bursting pressure, 350 and 533 rpm, respectively.

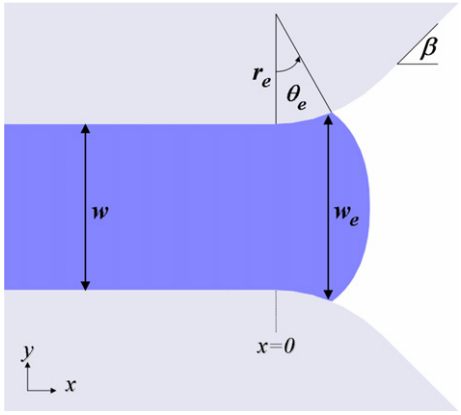

Fig. 11. A realistic description of the valve with round edges.

5. Summary

Capillary burst microvalves based on the diverging channel section had been suggested previously, but no rigorous theoretical explanation was devoted to their operations so far. Thus we have reported the theoretical analysis of the capillary burst valve to provide the maximum pressure difference that the valve can withstand. Such prediction requires the valve dimensions and the wetting properties of the liquid/solid combination. Therefore, there is no need to find fitting constants for each valve geometry as in the previous modeling approaches.

We conclude with summarizing the major concept lying behind our theory. The contact line can start to advance when the dynamic contact angle reaches the critical value. The capillary burst valve suddenly reduces the advancing contact angle to stop the flow until the interface bulges to reach the critical advancing contact angle with a diverging wall. The driving pressure difference should increase to bulge the interface. The valve geometry determines the critical pressure difference that can be resisted. We fabricated the microvalves of PDMS in this work and measured the bursting rotational speed. The experimental results were in reasonable agreement with the theoretical predictions. However, when the channel is very narrow, the valve tends to burst at a lower rotational speed than predicted, which is attributed to the imperfect valve shape of small sizes.

Acknowledgments

This work was supported by the Intelligent Microsystem Center sponsored by the Korea Ministry of Commerce, Industry and Energy through 21st century's Frontier Project. We thank Jong-In Hong and Heon Ju Lee for the help with the measurement of surface tensions and contact angles, respectively. H.Y.K. acknowledges administrative support from the Institute of Advanced Machinery and Design at Seoul National University.

References

[1] M.A. Burns, C.H. Mastrangelo, T.S. Sammarco, F.P. Man, J.R. Webster, B.N. Johnson, B. Foerster, D. Jones, Y. Fields, A.R. Kaiser, D.T. Burke, Proc. Natl. Acad. Sci. USA 93 (1996) 5556.
[2] A. Manz, H. Becker (Eds.), Microsystem Technology in Chemistry and Life Sciences, Springer-Verlag, Berlin, 1998.
[3] P.-A. Auroux, D. Iossifidis, D.R. Reyes, A. Manz, Anal. Chem. 74 (2002) 2637.
[4] D.R. Reyes, D. Iossifidis, P.-A. Auroux, A. Manz, Anal. Chem. 74 (2002) 2623.
[5] A. Ullmann, I. Fono, J. Microelectromech. Syst. 11 (2002) 655.
[6] C.-H. Chen, J.G. Santiago, J. Microelectromech. Syst. 11 (2002) 672.
[7] B. Zhao, J.S. Moore, D.J. Beebe, Anal. Chem. 74 (2002) 4259.
[8] D.C. Duffy, H.L. Gills, J. Lin, N.F. Sheppard, G.J. Kellogg, Anal. Chem. 71 (1999) 4669.
[9] S. Lai, S. Wang, J. Luo, L.J. Lee, S.-T. Yang, M.J. Madou, Anal. Chem. 76 (2004) 1832.
[10] H. Cho, H.-Y. Kim, J.Y. Kang, S.M. Kwak, T.S. Kim, KIEE Int. Trans. EA 4 (2004) 159.
[11] Y. Xia, G.M. Whitesides, Angew. Chem. Int. Ed. 37 (1998) 550.
[12] J.V. Zoval, M.J. Madou, Proc. IEEE 92 (2004) 140.
[13] R.L. Hoffman, J. Colloid Interface Sci. 50 (1975) 228.
[14] E.B. Dussan V., Ann. Rev. Fluid Mech. 11 (1979) 371.
[15] H.-Y. Kim, H.J. Lee, B.H. Kang, J. Colloid Interface Sci. 247 (2002) 372.
[16] J.W. Gibbs, Scientific Papers, vol. 1, Dover, New York, 1961, p. 326 (1906).
[17] J.F. Oliver, C. Huh, S.G. Mason, J. Colloid Interface Sci. 59 (1977) 568.